International Journal of Medical Toxicology & Forensic Medicine

January 2026, Volume 16, E50951

Research Paper

Determination of Postmortem Interval Using the Oxidative Stress Markers, Histopathological, Immunohistochemical, and Molecular Changes of Spleen, Pancreas, and Heart: Experimental study

Amani Abd El Fattah[1], Maha Ali Ahmed[1*], Dina Ali Shokry[1], Sara Adel Hosny[2], Zeinab A. Nour[3], Noha Maher Elrewieny[1]

1. *Forensic Medicine and Clinical Toxicology Department, Faculty of Medicine, Cairo University, Egypt.*
2. *Histology department, Faculty of Medicine, Cairo University, Egypt.*
3. *Medical Biochemistry &Molecular Biology Department-Faculty of Medicine, Cairo University, Egypt.*

Citation Abd El Fattah A, Ahmed MA, Shokry DA, Hosny SA, Nour ZA, Elrewieny NM. Determination of Postmortem Interval Using the Oxidative Stress Markers, Histopathological, Immunohistochemical, and Molecular Changes of Spleen, Pancreas, and Heart: Experimental study. International Journal of Medical Toxicology and Forensic Medicine. 2026;16:E50951.

https://doi.org/10.22037/ijmtfm.v16.50951

Article info:

Received: 02 Dec, 2025

First Revision: 12 Dec, 2025

Accepted: 19 Dec, 2025

Published: 01 Jan, 2026

Keywords:

Postmortem interval, BCL2, Molecular changes, Oxidative stress

ABSTRACT

Background: A cornerstone of forensic practice is determining the postmortem interval to resolve suspicious deaths and assist in criminal investigations. The work aims to estimate the postmortem interval (PMI) using oxidative stress markers, and to Assess Molecular, histopathological, and immunohistochemical changes in the spleen, pancreas, and heart of adult albino rats.

Methods: 30 adult albino rats were divided into five groups. All rats were sacrificed and kept at room temperature. Dissection of the spleen, pancreas, and heart was done at 0 (control), 6, 24, 48, and 72 hours. The following parameters were measured: malondialdehyde (MDA), reduced glutathione (GSH), superoxide dismutase (SOD), hypoxia-associated factor (HAF), apoptosis-inducing factor (AIF), and B-cell lymphoma 2 (BCL2) immunostaining.

Results: MDA, GSH, and SOD showed strong positive correlations with PMI in the pancreas, whereas in the heart, GSH showed a fair positive correlation with PMI.SOD showed a strong positive correlation with PMI in the spleen, while GSH showed a strong negative correlation with PMI. HAF showed a strongly significant positive association with PMI in the heart and the spleen, whereas in the pancreas, it showed a fair correlation. AIF showed a significant negative correlation with PMI in the heart. Histological changes showed time-dependent changes. BCL2 immunohistochemical expression showed a significant decrease over time in all organs.

Conclusion: Oxidative stress markers, Molecular, histopathological, and immunohistochemical changes can help estimate PMI. Four novel equations were developed to estimate PMI using the studied parameters across different organs.

*** Corresponding Author:**

Maha Ali Ahmed, MD

Forensic Medicine and Clinical Toxicology Department, Faculty of Medicine, Cairo University, Egypt.

E-mail: *maha.salim@kasralainy.edu.eg*

Introduction

Determining the period since death, or PMI, is a crucial component of forensic medicine. When examining the deceased corpse, this question is frequently asked [1].

In any forensic case, identifying the time of death is an important issue. In both civil and criminal cases, it is essential to calculate the PMI effectively. The PMI assists in identifying and excluding suspects, determining the exact time of a crime, and resolving legal matters related to inheritance [2].

The body of the deceased undergoes a series of physical and chemical changes immediately after death. These changes are inevitable, irrevocable, and progressive. Understanding postmortem processes and the factors that affect them can help estimate the PMI [3].

Many biological elements, such as deoxyribonucleic acid (DNA), messenger ribonucleic acid (mRNA), and proteins, are chemically and physically damaged by putrefaction as the postmortem interval increases, and this can be used to estimate the time of death [4].

A combination of histology and immunohistochemistry has been used to identify morphological features in tissues and assess the expression of marker proteins to establish the time of death [5].

After death, it is not possible to believe that the body can maintain an effective balance between oxidants and antioxidants. Consequently, variations in oxidant/antioxidant parameters are considered biochemical disturbances [6].

Materials and Methods

Study design

The research was conducted in the Animal House at the Faculty of Medicine, Cairo University, and involved 30 adult male albino rats weighing 180-200 grams, housed under normal light/dark cycles and free access to food and water. After 1 week of acclimatization, the rats were randomly assigned to 5 groups, each with 6 rats. All the rats were sacrificed through spinal dissection and kept at a normal room temperature of 22.25C°. The spleen, pancreas, and heart were carefully dissected at 0, 6, 24, 48, and 72 hours after death. Half of the spleen, pancreas, and heart were frozen at -80°C for molecular and oxidative marker measurements. For histological and immunohistochemical examination, the other half of the heart, pancreas, and spleen were preserved in a 10% neutral formalin solution.

Measurement of Oxidative Stress Markers

The tissue levels of MDA, GSH, and SOD were determined using commercial kits from the Biodiagnostic Company, Egypt, with the following catalog numbers: MD 25 29 for MDA, GRTA 25 11 for GSH, and SD 25 21 for SOD. The weight of the tissue samples was recorded, and they were then ground and handled according to the manufacturer's instructions.

Molecular Study

Real-time PCR for HAF, AIF gene expression (Table 1).

Table 1. The primer sequence of the studied gene.

Gene		Primer sequence
HAF	Forward	GTGAAAGACCATTGCAGC
	Reverse	TTTCCCAGTGAGGTGTTC
AIF	Forward	CAATCAGTTGGAGTCAGC
	Reverse	TACCTTCCTTCCATCTTT

International Journal of Medical Toxicology & Forensic Medicine

RNA extraction: Total RNA from each tissue sample was extracted using an RNA extraction kit (Favorgen Biotech Corp., Taiwan; catalog number FATRK 001).

ß-Mercaptoethanol and buffer were added to a 30 mg tissue. After incubation and centrifugation (18,000xg) for 2 minutes, the supernatant was transferred to a new tube, where ethanol was added, then centrifuged at (18,000xg) for 2 minutes in a new mini column and collection tube. Three rounds of centrifugation with added wash buffer and flow-through discarding were performed; the final round was performed after adding 50 µL of RNase-free H2O to an elution tube, to which the resultant RNA was added, and the mixture was stored at -80°C.

Reverse Transcription (RT): The extracted RNA was used as a template for reverse transcription into complementary DNA (cDNA) using a cDNA reverse transcription kit (ELK biotech, USA). (Cat. No. EQ010). A 25 ul mix of RT Primer mix, dNTPs, reverse transcriptase, RNase inhibitor, RNase-free H2O, and RNA template was heated to 37°C for 1 hour, followed by 95°C for 5 minutes to inactivate reverse transcriptase.

Real-Time qPCR: Real-time quantitative polymerase chain reaction (qPCR) amplification and analysis were performed using ViPrimePLUS Taq qPCR Green Master Mix I (SYBR® Green Dye), Malaysia, code: QLMM12. A final 20 ul mix of Taq polymerase master mix, cDNA, primers (Table 1), and nuclease-free water was subjected to enzyme activation at 95°C for 2 minutes, followed by 45 thermal cycles of 15 seconds at 95°C and 60 seconds at 60°C using a thermal cycler (Step One Applied Biosystem, Foster City, USA). Relative expression (RQ) for each sample was estimated using the 2− ΔΔCt method.

Histopathological Study

Hematoxylin and Eosin stain [7]. After scarification, the organs were dissected, fixed in 10% formalin saline, washed, dehydrated, cleared, and embedded in paraffin for histological study. Sections 5µm thick were cut and stained with H&E.

Immunohistochemical staining [8].

Materials (kits) supplied: Primary antibodies: Anti Bcl-2 antibody, it is a polyclonal (Human, mouse, rat) antibody (Chongqing Biospece. China. Cat. No YPA1386).

Steps of Immunohistochemical Staining: Sections were deparaffinized, rehydrated, and heated in 10 mM citrate buffer (pH 6) for 30 minutes to prepare them for immunohistochemical labeling. Following that, the sections were incubated overnight with primary antibodies in a humidity chamber. The DAB HRP Brown Detection System multi-detector for mice and rabbits (Bio SB, China, Cat. # BSB 0201S) was incubated at room temperature for 45 minutes in a humidity chamber. The immunohistochemical staining process utilized Mayer's hematoxylin as a counterstain and aminobenzidine as a chromogen.

Statistical analysis

IBM Corp.'s Statistical Program for the Social Sciences, version 28 (Armonk, NY, USA), was used to code and enter the data. The mean and standard deviation were used to summarize the data. For regularly distributed quantitative variables, groups were compared using analysis of variance (ANOVA) with a post hoc multiple-comparison test; for non-normally distributed quantitative variables, the nonparametric Mann-Whitney and Kruskal-Wallis tests were used [9].

The Spearman correlation coefficient was used to determine correlations between quantitative variables [10]. Using various parameters, PMI was predicted via linear regression. P-values are considered to be statistically significant if they are less than 0.05 [11].

Results

Oxidative Stress Markers

In the present study, the levels of the oxidative stress markers in various tissues showed significant changes with postmortem interval, as illustrated in Table 2.

In the pancreas, MDA, GSH, and SOD showed statistically significant differences across the studied groups, with values gradually increasing over time. The highest levels were observed in the 72-hour group after death.

Table 2. Comparison of oxidative stress markers in different groups.

	Group 1 (control) (0 h)	Group 2 (6 h)	Group 3 (24 h)	Group 4 (48 h)	Group 5 (72 h)	P value
MDA (Pancreas)	16.32±11.54	35.37±17.64	46.39±7.66	57.14±37.02	92.86±56.08 *#	0.005
GSH (Pancreas)	8.89±3.47	19.11±15.35	18.11±18.05	53.55±39.2	124.88±46.55 *#$@	<0.001
SOD (Pancreas)	1968.58±167.62	1837.5±238.23	2031.21±121.15	2131.35±33.12 #	2172.31±43.85 #	0.003
MDA (Spleen)	87.35±23.64	222.04±42.88 *	183.4±31.92 *	137.55±42.05 #	49.32±40.26 #$@	<0.001
GSH (Spleen)	15.44±7.12	24.89±10.46	11.28±5.71 #	9±2.75 #	2.22±3.44 *#	<0.001
SOD (Spleen)	1343.71±95.71	1219.38±76.13	2178.06±23.33 *#	2228.06±19.84 *#	1749.92±234.71 *#$@	<0.001
MDA (Heart)	64.76±39.75	88.64±41.74	105.03±30.98	169.12±40.62 *#	61.43±39.06 @	<0.001
GSH (Heart)	7±0.7	22.22±6.42 *	11.22±3.3 #	15.55±3.36 *	15.66±2.91 *	<0.001
SOD (Heart)	1784.36±224.26	1719.38±202.51	1690.34±126.06	1656.58±207.56	1688±260.66	0.862

International Journal of Medical Toxicology & Forensic Medicine

Values are presented as mean ±SD
*: statistically significant compared to the corresponding value in group I (P<0.05)
#: statistically significant compared to the corresponding value in group II (P<0.05)
$: statistically significant compared to the corresponding value in group III (P<0.05)
@: statistically significant compared to the corresponding value in group IV (P<0.05)

Regarding the heart, MDA and GSH levels varied significantly among the study groups (p-value < 0.001). MDA increased over time, reaching its peak at 48 hours. GSH levels were low at the time of death (0h group) and then increased to their maximum level in the 6-hour group. SOD level wasn't statistically significant among the studied group.

In the spleen, MDA and GSH levels were highest in the 6-hour group and then gradually decreased. SOD levels increased progressively, with the 48-hour group showing the highest value, indicating a statistically significant difference between the groups.

In the pancreas, MDA, GSH, and SOD showed strong positive correlations with the postmortem interval. In the heart, a fair positive correlation was present between GSH and PMI. In the spleen, SOD showed a strong positive correlation with PMI, while GSH showed a strong negative correlation with PMI (Table 3).

Table 3. Spearman Correlation coefficient for the correlation between the time after death (PM interval) and analyzed oxidative stress markers in the different tissues.

	PMI (Hrs)		
	Correlation Coefficient	P value	N
MDA (Pancreas)	0.624	<0.001	30
GSH (Pancreas)	0.683	<0.001	30
SOD (Pancreas)	0.662	<0.001	30
MDA (Spleen)	-0.277-	0.139	30
GSH (Spleen)	-0.693-	<0.001	30
SOD (Spleen)	0.601	<0.001	30
MDA (Heart)	0.148	0.434	30
GSH (Heart)	0.367	0.046	30
SOD (Heart)	-0.171-	0.368	30

International Journal of Medical Toxicology & Forensic Medicine

Molecular Markers

As shown in Table 4**, regarding AIF expression in the pancreas, heart, and spleen, there was a highly statistically significant difference between the groups (p-value <** 0.001). The maximum expression occurred at the time of death in both the pancreas and the heart, whereas in the spleen it occurred at 24 h post-death. In the heart and spleen, HAF showed a highly significant difference between the two studied groups (p-value < 0.001). The mean expression value was low at the time of death, then gradually increased, whereas in the pancreas, there was no statistically significant difference.

HAF demonstrated a statistically significant positive correlation with the PMI in both the heart and the spleen (p-value <0.001), whereas in the pancreas, it showed a fair correlation (p-value 0.019). In the heart, AIF and PMI showed a highly significant negative correlation (p-value < 0.001), whereas in the pancreas and spleen, the correlation was non-significant (Table 5).

Table 5. Spearman Correlation between PMI and AIF & HAF in the pancreas, spleen, and heart.

	PMI (Hrs)		
	Correlation Coefficient	P value	N
AIF (Pancreas)	-0.143-	0.450	30
HAF (Pancreas)	0.426	0.019	30
AIF (Heart)	-0.707-	<0.001	30
HAF (Heart)	0.848	<0.001	30
AIF (Spleen)	0.115	0.546	30
HAF (Spleen)	0.643	<0.001	30

International Journal of Medical Toxicology & Forensic Medicine

BCL2 Immunostaining

There was a highly statistically significant difference in the mean BCL2 optical density of the spleen, pancreas, and heart between the groups under study (p-value <0.001), as shown in Table 6. BCL2 immunostaining showed a very strong, highly significant negative correlation with postmortem interval in the pancreas, spleen, and heart, respectively

Table 4. Comparison between the relative expression of AIF and HAF within the studied groups in different organs using Post hoc pairwise tests.

	0 h-Group (control)	6 h-Group	24 h-Group	48 h-Group	72 h-Group	P value
AIF (Pancreas)	1±0	0.01±0 *	0.02±0.01 *	0.05±0.06*	0.15±0.06*#$@	**<0.001**
HAF (Pancreas)	1±0.01	1.34±0.51	2.09±1.35	2.34±1.24	1.64±0.89	**0.123**
AIF (Heart)	1.09±0.48	0.46±0.33*	0.22±0.16 *	0.1±0.06 *	0.11±0.1 *	**<0.001**
HAF (Heart)	1.04±0.25	1.74±0.84	4.72±1.1	13.82±7.26*#$	12.26±6.36 *#	**<0.001**
AIF (Spleen)	1±0.01	0.47±0.17	4.97±1.29*#	0.24±0.26 $	2.42±0.82*#$@	**<0.001**
HAF (Spleen)	1.02±0.04	7.47±2.12*	3.84±2.63	8.69±5.25 *	9.14±3.06*	**<0.001**

International Journal of Medical Toxicology & Forensic Medicine

Values are presented as mean ±SD
*: statistically significant compared to corresponding value in group I (P<0.05)
#: statistically significant compared to corresponding value in group II (P<0.05)
$: statistically significant compared to corresponding value in group III (P<0.05)
@: statistically significant compared to corresponding value in group IV (P<0.05)

Table 6. Comparison of optical density of BCL2 within the studied groups in different organs using the post hoc pairwise test.

	0 h-Group (control)	6 h-Group	24 h-Group	48 h-Group	72 h-Group	P value
BCL2 (Pancreas)	23.73±1.65	18.68±1.43*	11.4±1.22*#	6.93±0.99 *#$	4.5±0.68*#$@	**<0.001**
BCL2 (Heart)	32.57±1.31	27.62±1.39*	23.87±1.04*#	15.23±1.22*#$	9.58±1.11*#$@	**<0.001**
BCL2 (Spleen)	19.72±1.11	15.17±1.17*	12.62±0.79*#	8.37±0.57 *#$	6.17±0.57*#$@	**<0.001**

Values are presented as mean ±SD
*: statistically significant compared to the corresponding value in group I (P<0.05)
#: statistically significant compared to the corresponding value in group II (P<0.05)
$: statistically significant compared to the corresponding value in group III (P<0.05)
@: statistically significant compared to the corresponding value in group IV (P<0.05)

Table 7. Spearman Correlation between PMI and optical density of BLC2 in pancreas, spleen and heart.

	PMI (Hrs)		
	Correlation Coefficient	P value	N
BCL2 (Pancreas)	-0.980-	<0.001	30
BCL2 (Heart)	-0.980-	<0.001	30
BCL2 (Spleen)	-0.978-	<0.001	30

Table 7.

Histopathological

Regarding the pancreas, pancreatic sections from the 0 h group showed acini with basophilic cytoplasm, pale, vesicular nuclei, and apical granular acidophilic cytoplasm. Centroacinar cells were seen at the centers of the acini. Examination of the 6h-group demonstrated pancreatic acini with pale, basally located nuclei and apical acidophilic granular cytoplasm.

Some acini were shrunken with dark nuclei. The 24h-group showed a few widely separated acini, some of which were shrunken with dark nuclei, and others

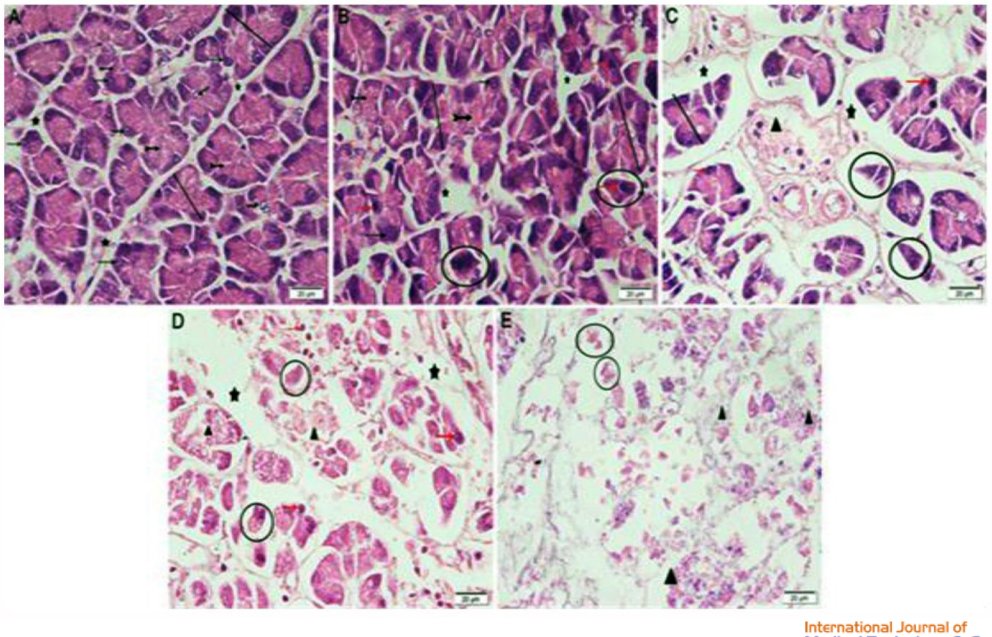

Figure 1. A Photomicrograph of Pancreatic sections (x400), A) 0 h-group demonstrating Acini (line) having basal basophilic cytoplasm with pale vesicular nuclei (arrows) and apical acidophilic granular cytoplasm (bifid arrows). Note the presence of Centro acinose cells in the center of acini (wavy arrows) with connective tissue septum in-between (Astrex). B) 6 h-group showing pancreatic acini (line) with basal pale nuclei (arrows) and apical acidophilic granular cytoplasm (bifid arrows). Some acini are shrunken (circle) with dark nuclei (red arrows). Note widened areas in the connective tissue septum (Astrex). C) 24 h-group revealing few acini (lines) widely separated by connective tissue (Astrex). Some Acini are shrunken (circle) with dark nuclei (red arrows) and others are degenerated (▲). D) 48 h-group exhibiting large areas of degenerated acini (▲) among few shrunken acini (circle) having dark nuclei (red arrows). Note the presence of wide spaces (Astrex) in between the degenerated cells. E) 72 h-group showing degenerated acini (▲) among few shrunken acini (circle) with no nuclei.

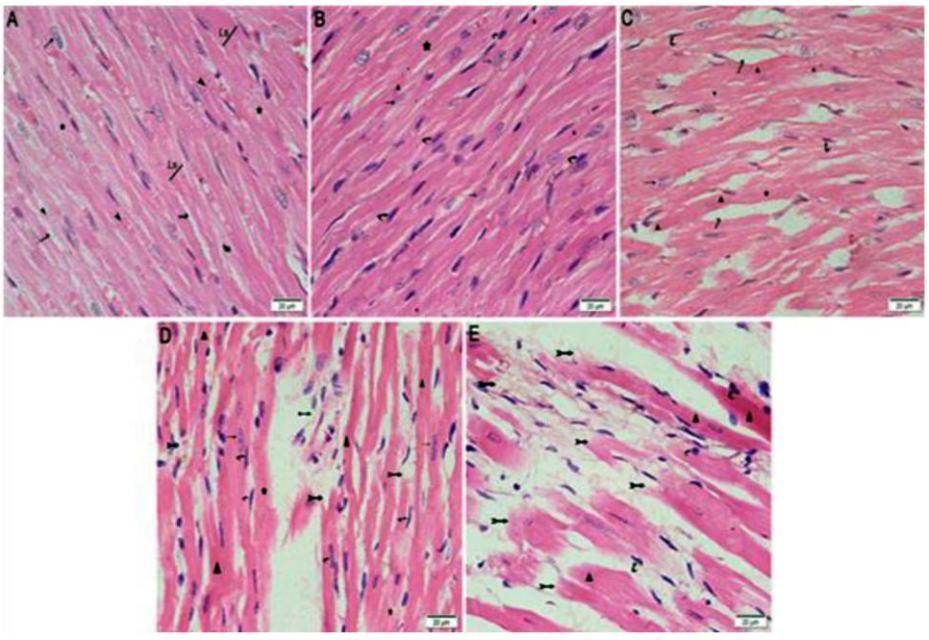

Figure 2. A Photomicrograph of Longitudinal sections in the cardiac muscle (x400), A) 0 h-group exhibiting longitudinal branching fibers (Ls) having pale central nuclei (arrows) and striated cytoplasm (Astrex) with intercalated discs. (arrowheads). Note the presence of thin connective tissue (wavy arrows) in between the fibers. B) 6 h-group revealing longitudinal fibers having pale central nuclei (arrows) with some dark pyknotic nuclei (curved arrows). The cytoplasm shows acidophilic homogenous areas (▲) among areas of transverse striations (Astrex). C) 24 h-group showing cardiac muscle fibers widely separated with connective tissue endomysium (wavy arrows). Some fibers reveal dark homogenous cytoplasm (▲) among areas with transverse striations (Astrex). Most nuclei are pale vesicular (arrows) with few dark pyknotic nuclei (curved arrows). D) 48 h-group revealing areas of degenerated cardiac muscle fibers (bifid arrows). Most the cytoplasm is dark homogenous (▲) among few areas with transverse striations (Astrex). The fibers contain many dark pyknotic nuclei (curved arrows) with few pale nuclei (arrows). E) 72 h-group exhibiting large areas of degenerated muscle fibers (bifid arrows) with dark homogenous cytoplasm (▲). Most nuclei are dark pyknotic (curved arrows).

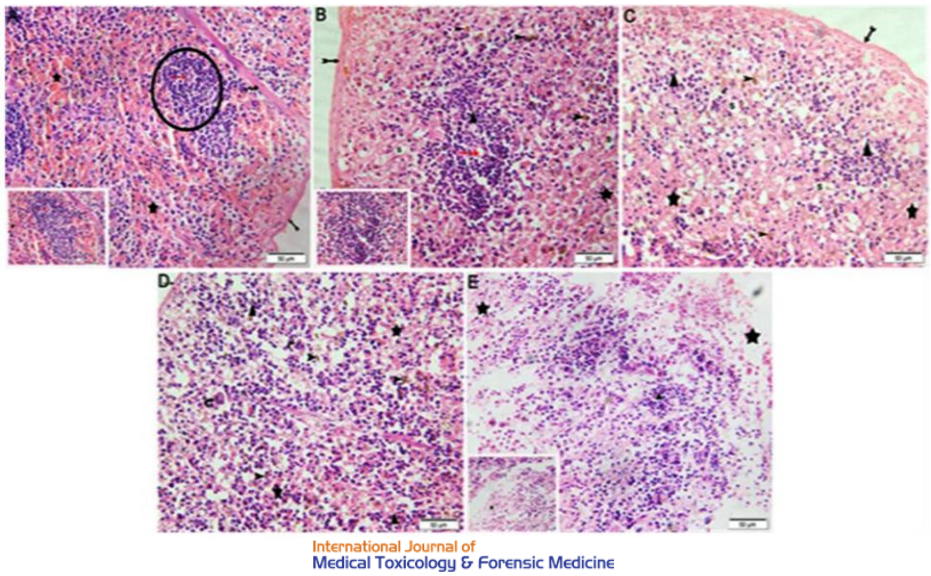

Figure 3. A Photomicrograph of Splenic sections (x200, inset x400), A) 0 h-group exhibiting splenic stroma formed of capsule (bifid arrows) with trabeculae (wavy arrows) descending from it. The splenic parenchyma formed of red pulp (Astrex) and white pulp (circle) having central arteriole (red arrow). B) 6 h-group demonstrating thickened capsule (bifid arrow). Dispersed lymphocytes of white pulp (▲) among expanded congested red pulp (Astrex). Note the presence of central arteriole (red arrow) in the degenerated white pulp. Dilated blood sinusoids (S) and hemosiderin granules in between the RBCs and lymphocytes can be seen. C) 24 h-group showing widely dispersed lymphocytes (▲) among the red pulp (Astrex) and hemosiderin pigments in many cells (arrow heads). Note the thinning of capsule (bifid arrow) and dilatation of blood sinusoids (S). D) 48 h-group revealing widely dispersed lymphocytes (▲) among the red pulp (Astrex) and hemosiderin pigments in many cells (arrow heads). Note the presence of thin capsule (bifid arrow). Multinucleated cells (curved arrows) can be seen. E) 72 h-group reveals degenerated splenic parenchyma with widely dispersed lymphocytes (▲) and RBCs (Astrex).

were degenerated. Furthermore, the 48h and 72h groups showed large areas of degenerated acini, along

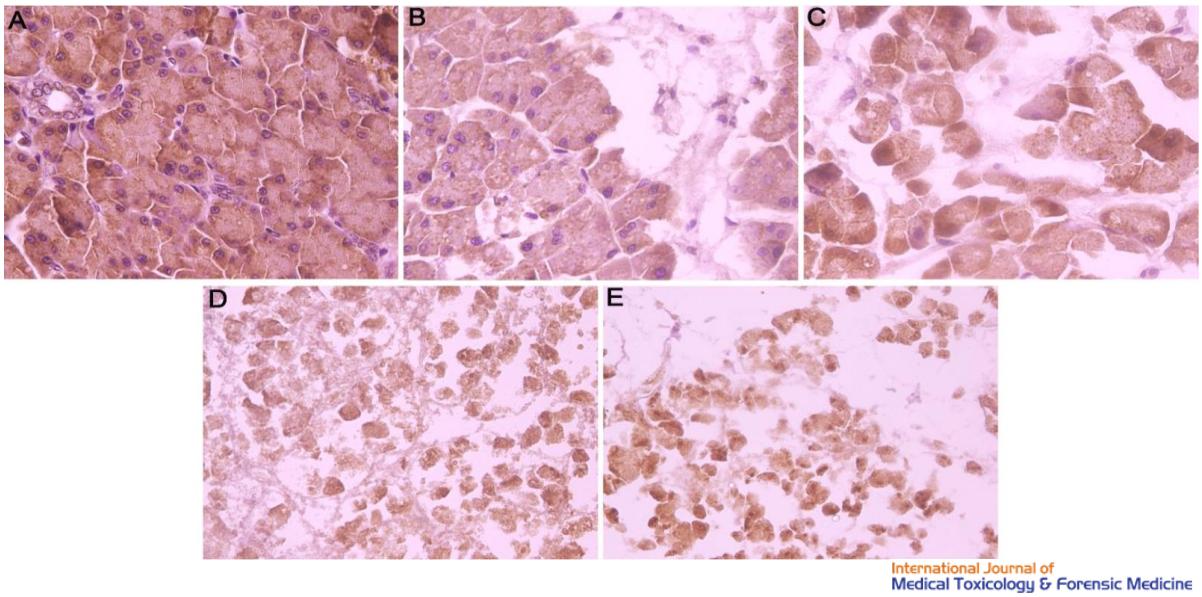

Figure 4. A photomicrograph of Pancreatic sections immunostained by BCL-2 (x400), A) 0 h group: Pancreatic acini are darkly stained with BCL-2. B) 6 h-group: Acini shows moderate BCL-2 immunostaining. C) 24 h-group: Most of the acini are pale stained among few moderately stained acini. D) 48 h-group: Acini revealed decreased immunostaining with BCL-2. E) 72 h-group: The remanent cells exhibited faint BCL-2 immunostaining.

with a few shrunken acini with dark nuclei or no nuclei (Figure 1).

Regarding the heart, examination of longitudinal sections of the cardiac muscle in the 0 h group revealed branching fibers with pale central nuclei, striated cytoplasm, and intercalated discs. Thin connective tissue was observed between the fibers. Additionally, the 6h-group showed longitudinal fibers with some dark pyknotic nuclei among the pale nuclei. Some areas of the cytoplasm appeared acidophilic and homogenous. The 24h-group exhibited cardiac muscle fibers with dark, homogeneous cytoplasm, widely separated by the connective tissue endomysium.

Most nuclei were pale vesicular, with a few dark pyknotic nuclei. Furthermore, the 48h-group demonstrated areas of

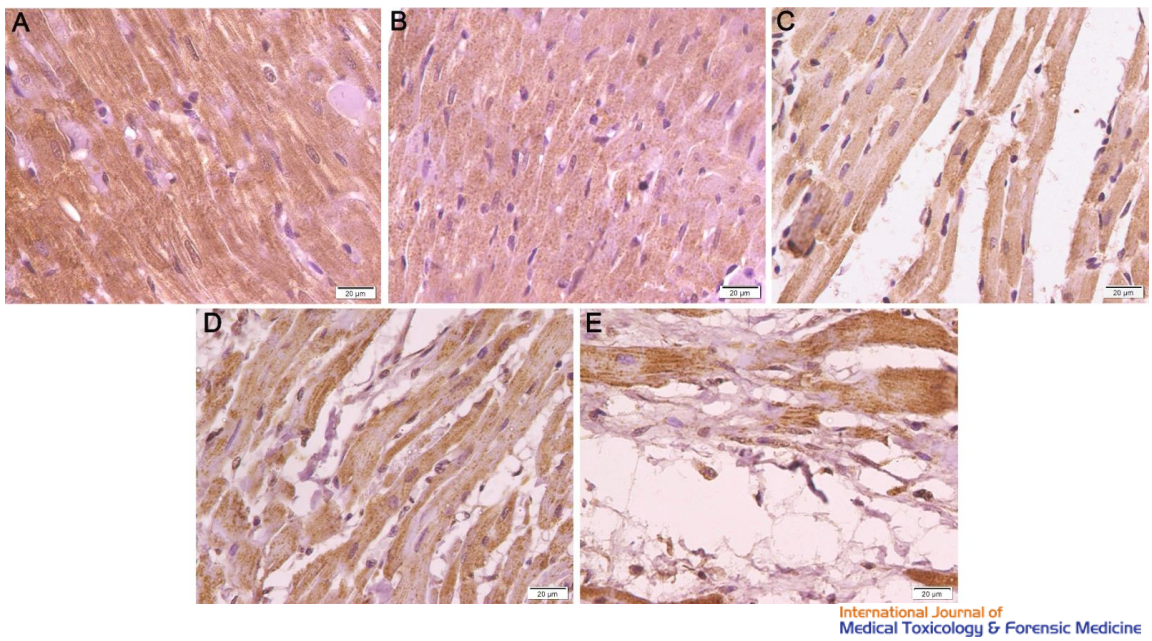

Figure 5. A photomicrograph of BCL-2 immunostained cardiac sections (x4400), A) 0h-group: Cardiac fibers reveal intense positive BCL-2 immunostaining. B) 6 h-group: Fibers exhibit moderate BCL-2 immunostaining. C) 24h-group: Degenerated fibers show mild BCL-2 immunostaining among areas of moderate immunostaining. D) 48h-group: Most of the fibers are pale stained with BCL-2. E) 72h-group: The remanent of fibers are faintly immunostained with BCL-2.

Table 8. Multivariate linear regression to predict PMI in Pancreas, heart and spleen separately.

Model		Unstandardized Coefficients		Standardized Coefficients	t	P value	95.0% Confidence Interval for B	
		B	Std. Error	Beta			Lower Bound	Upper Bound
PMI pancreas	(Constant)	57.594	4.675		12.319	**<0.001**	48.002	67.187
	BCL2 (Pancreas)	-2.686-	0.248	-0.730-	-10.815-	**<0.001**	-3.196-	-2.177-
	GSH (Pancreas)	0.166	0.036	0.312	4.629	**<0.001**	0.093	0.240
PMI Heart	(Constant)	107.187	3.383		31.679	**<0.001**	100.245	114.129
	BCL2 (Heart)	-3.229-	0.100	-1.011-	-32.299-	**<0.001**	-3.434-	-3.024-
	GSH (Heart)	-0.480-	0.136	-0.110-	-3.516-	**0.002**	-0.760-	-0.200-
PMI Spleen	(Constant)	93.849	3.744		25.065	**<0.001**	86.167	101.532
	BCL2 (Spleen)	-4.534-	0.339	-0.826-	-13.381-	**<0.001**	-5.229-	-3.839-
	GSH (Spleen)	-0.605-	0.173	-0.216-	-3.494-	**0.002**	-0.960-	-0.250-

degenerated cardiac muscle fibers with dark, homogeneous cytoplasm. The fibers contained many dark pyknotic nuclei and few pale nuclei. Lastly, the 72h-group showed large areas of degenerated muscle fibers with dark, homogeneous cytoplasm and dark, pyknotic nuclei (Figure 2).

Regarding the spleen, the 0-hour group demonstrated a splenic stroma composed of a capsule with descending trabeculae. The splenic parenchyma consisted of red pulp and white pulp with a central arteriole. Additionally, the 6-hour and 24-hour groups showed dispersed lymphocytes in the white pulp among an expanded, congested red pulp. It is crucial to observe the presence of a central arteriole within the degenerated white pulp. Hemosiderin pigments could be detected in many cells along with dilated blood sinusoids. In the 48-hour group, multinucleated cells appeared in many areas. Furthermore, the 72-hour group exhibited degenerated splenic parenchyma with widely dispersed lymphocytes and red blood cells (Figure 3).

BCL-2 immunohistochemical Results: In the pancreas, the 0 h group showed darkly immunostained acini for BCL-2; the 6 h group showed many acini with intense BCL-2 immunostaining, with few moderate-stained acini. In the 24 h group, moderate BCL-2 immunostaining was observed in the degenerated acini. Moreover, the 48 h and 72 h groups

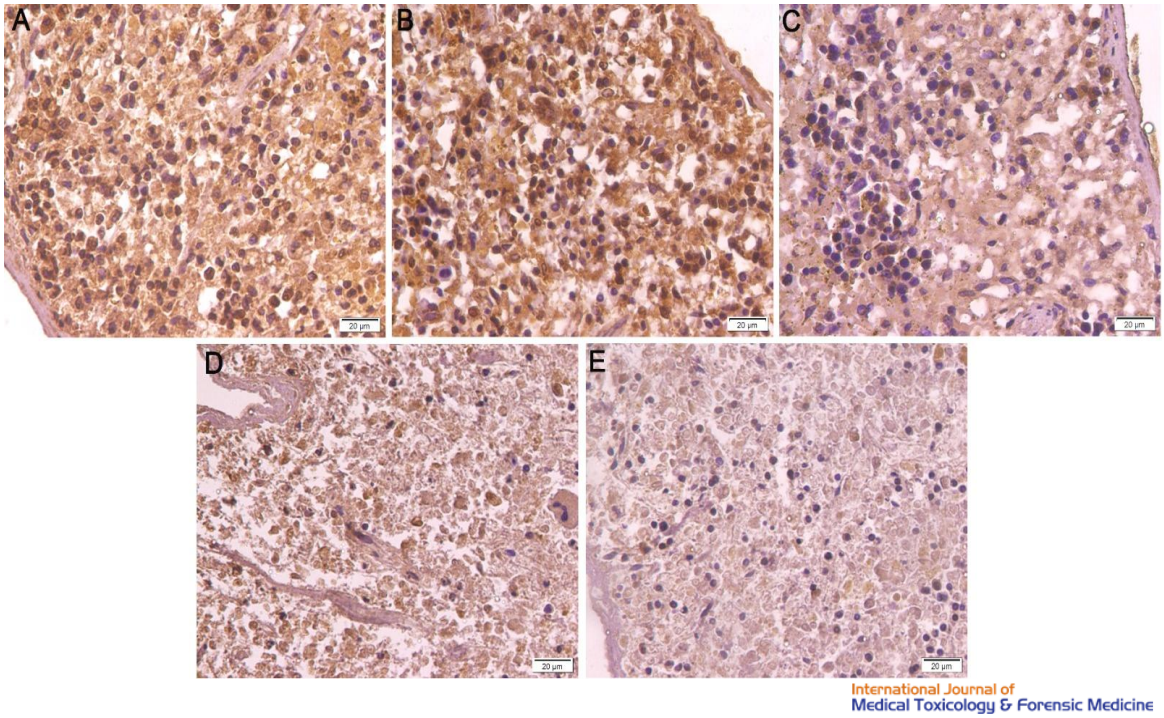

Figure 6. A photomicrograph of BCL-2 immunostained cardiac sections (x4400), A) 0h-group: Cardiac fibers reveal intense positive BCL-2 immunostaining. B) 6 h-group: Fibers exhibit moderate BCL-2 immunostaining. C) 24h-group: Degenerated fibers show mild BCL-2 immunostaining among areas of moderate immunostaining. D) 48h-group: Most of the fibers are pale stained with BCL-2. E) 72h-group: The remanent of fibers are faintly immunostained with BCL-2.

showed a significant decrease in optical density of BCL-2 immunostaining in the remaining cells (Figure 4).

Furthermore, the cardiac muscle of the 0 h-group showed intense, widespread positive BCL-2 immunostaining in all fibers, while the 6 h-group revealed moderately stained fibers with BCL-2. Optical density of BCL-2 immunostaining is significantly decreased in degenerated cardiac muscles of 24h and 48h-groups. At the same time, the 72 h-group exhibited faint BCL-2 immunostaining in the remnant muscle fibers (Figure 5).

In addition, the splenic cells exhibited intense, widespread brownish BCL-2 immunostaining, which insignificantly decreased in the 6 h group. Furthermore, the 24 h and 48 h groups showed significant decreases in BCL-2 immunostaining. Finally, the remanent splenic cells demonstrated faint BCL-2 immunostaining (Figure 6).

Four novel equations were constructed to estimate the PMI using the studied parameters in the different organs: An equation was constructed using all statistically significant parameters in the pancreas by multivariate linear regression analysis, and a statistically significant correlation was revealed between BCL2 and GSH (p value<0.001 in both), with PMI (Table 8).

PMI=57.594-2.686* BCL2 (Pancreas) +0.166* GSH (Pancreas)

Regarding the heart, all statistically significant parameters were combined in a multivariate linear regression analysis. Statistically significant correlations between BCL2 and GSH and between BCL2 and PMI (p values < 0.001 and < 0.001, respectively) were found. These correlations were used to develop an equation for estimating PMI. (Table 8).

PMI=107.187-3.229* BCL2 (Heart) -0.480* GSH (Heart)

The statistically significant parameters in the spleen were combined in a multivariate linear regression analysis. Statistically significant correlations were observed between BCL2 and GSH and between BCL2 and PMI (p values < 0.001 and 0.0012, respectively). These correlations were used to develop an equation for estimating PMI (Table 8).

PMI=93.849-4.534* BCL2 (spleen) -0.605* GSH (Spleen)

All statistically significant parameters were included in a multivariate linear regression analysis, and only BCL2 (heart) and GSH (spleen) showed statistically significant correlations with the postmortem interval. These correlations were used to develop an equation for estimating PMI (Table 9).

PMI=97.434-2.838* BCL2 (Heart) -0.449* GSH (Spleen).

Discussion

After death, a complex series of biochemical and pathological processes is triggered, leading to substantial changes in the structure and composition of the human body. It has been proposed that, because many of these changes occur in sequence, assessing the types and extent of changes may allow estimation of the time since death [12].

We aimed to study the correlation between the postmortem interval and alterations in oxidative stress markers, as well as histopathological, immunohistochemical, and molecular changes in the spleen, pancreas, and heart of rats within the first 72 hours after death.

In the present study, MDA showed a strong positive correlation with PMI in the pancreas. This result is in line with the findings of Welson et al. [13], who investigated MDA levels in rats' testes, hearts, and kidneys. It also aligns with Shaaban et al. [14], who reported a statistically significant positive association between time since death and the oxidant (MDA) in rat liver and brain tissues. Additionally, ElNoor et al. [6] investigated oxidant/antioxidant parameters to estimate the early postmortem interval in rat kidney and heart tissues [6].

A statistically significant, strong positive correlation between time since death and the investigated oxidant parameters (NO and MDA) in rat prostate was reported by Ali & Ahmed [15]. The increased MDA levels with advancing PMI could be explained by increased lipid peroxidation due to hypoxia [14].

GSH showed a statistically significant, strong negative correlation with PMI in the spleen. This finding was consistent with Mostafa et al. [16], who studied oxidant/antioxidant parameters in rat skeletal muscle and reported a highly significant negative correlation between time since death and antioxidant markers [16]. Additionally, Ali & Ahmed reported a strong negative correlation between postmortem time and GSH in prostate tissues that was statistically significant [15]. El Noor et al. [6] found that glutathione reductase was among the key factors affecting the estimation of early PMI in rat kidneys, findings consistent with ours [6]. GSH showed a statistically significant positive correlation with PMI in both

pancreatic and cardiac tissue. Variations in the nature, amount, and activity of these enzymes within organs could account for differences in enzyme responses [17].

Da Fonseca et al. [18] studied the PMI in relation to glutathione S-transferase (GST) activity in the brain, liver, kidney, and skeletal muscle tissues of male adult Swiss mice [18]. They found that the highest renal GST activity after death occurred at 48 hours, consistent with the results in the pancreas and heart. GST facilitates the conjugation of toxic compounds to GSH, thereby protecting cells against oxidative damage [14].

We found that SOD was significantly positively correlated with time since death in the pancreas and spleen of rats. In heart, the correlation was non-significant, which aligns with Shaaban et al. [14] ,who found a non-significant correlation between SOD and PMI in liver tissue.

In our study, the elevated SOD level in the pancreas may indicate a protective response of acinar cells to oxidative stress or pro-apoptotic stimuli [19]. Similarly, the spleen may reflect splenocytes' defensive response to oxidative stress.

SOD consists of a group of antioxidant enzymes that protect against free radicals. SOD exists in two forms: Cu/Zn SOD (SOD1), located in the cytosol, and SOD2, found in the mitochondria. The rise in SOD activity within the pancreas may be attributed to the fact that hypoxia increases the expression of superoxide dismutase 1 and 2, which in turn enhances superoxide dismutase activity [20].

SOD serves as the initial barrier against oxygen-derived free radicals by catalyzing the conversion of superoxide anion to hydrogen peroxide. This hydrogen peroxide can be changed into oxygen and water by catalase. SOD activity reflects the cell's ability to scavenge and eliminate free radicals [21]. Concerning the relative expression of AIF, our results found a statistically significant difference between the relative expression of AIF within the studied time intervals in the pancreas, spleen, and heart, and a significant negative correlation with PMI in heart tissue.

This was in agreement with the findings of Peng et al. 2020 [23], they used mRNA markers associated with cell oxygen deprivation and apoptosis as target genes, such as HAF, AIF, hypoxia-inducible factor 2 alpha (HIF2a), and factor inhibiting HIF (FIH), to examine the relationship between RNA quantity and PMI in the heart and brain of a mouse model over a 0–48 h PMI with 29 time points. They found that the expression levels of HIF2a-S, HIF2a-L, AIF, and FIH in heart tissue decreased after death, with P values indicating significant correlations with PMI at 0–48 h. Regarding the relative expression of HAF, the present study found a strong positive correlation with PMI in the pancreas, spleen, and heart, and a statistically significant difference in HAF expression across the time intervals studied in the spleen and heart.

Our findings are consistent with those of Bai et al. 2017 [23], who examined the expression level of HAF mRNA in the mouse brain tissue at 48 h PMI. They utilized RT-PCR to determine the expression levels of HAF mRNA and Caspase-3 DNA (the reference gene). They discovered a progressive increase in HAF mRNA throughout the entire observation period.

Earlier involvement of HAF mRNA in hypoxia-induced expression has been reported, so its elevated level after death may be due to hypoxic stimulation from cervical dislocation [23]. Peng et al. 2020 [22] found that HAF expression increased in brain tissue, whereas in heart tissue, no obvious changes were observed; in contrast, the levels of other mRNAs, such as the HIF2a marker, diminished over time postmortem. The autolytic process affects cell size, appearance, electron density, and localization, gradually disintegrating highly organized cell structures [24].

Our results were consistent with those of El Noor et al. [6], who found that anoxic postmortem effects that develop after death were responsible for the observed histological alterations. Enzyme activity and cellular structure are altered by these effects, leading to an autolytic process that modifies the size, shape, electron density, and localization of cellular structures. As this process continues, the cells' highly organized structural arrangement is lost. After death, lysosomal autolytic enzymes break down cellular components. These enzymes rapidly break down intracellular components, such as organelles, leading to a cytoplasm that is both homogeneous and highly eosinophilic. This eventually leads to the loss of details about cell and tissue architecture.

Welson et al. [13] reported similar changes in the hearts, kidneys, and testes of rats, but with a longer PMI of 120 hours. Similarly, Tomita et al. [25] found comparable findings in the heart and pancreas of rats within a 24-hour postmortem interval. Concerning BCL2 immunohistochemical staining, a statistically significant difference between the studied time intervals was revealed; moreover, BCL2 showed a strong, significant negative correlation with PMI.

The cardiac muscle showed intense, widespread

positive BCL-2 immunostaining in all fibers at the time of death (0h); the immunostaining decreased with time and became faint 72h postmortem. In addition, the pancreas in the control group (0h) revealed darkly immunostained acini for BCL-2; at 6h, many acini showed intense BCL-2 immunostaining, with few moderately stained acini; then, a gradual decrease in immunostaining and BCL-2 optical density was observed, with a significant decrease at 48 h and 72h postmortem. Furthermore, the splenic cells exhibited intense, widespread brownish BCL-2 immunostaining, which decreased significantly by 6 h. Finally, the remanent splenic cells demonstrated faint BCL-2 immunostaining.

This was consistent with the findings of Mohamed et al. [26], who investigated the microarchitecture and immunohistochemistry (p53 & BCL2) of white New Zealand rabbit brain tissue at different postmortem intervals (0, 6, and 12 hours PM) following traumatic brain injury, they reported a rise in the expression of apoptotic inducer (p53) with increasing PMI beginning at 6 h and intensifying in the 12 h groups. In contrast, the expression of the apoptotic inhibitor (Bcl-2) diminished correspondingly and became patchy in the 6-h and 12-h groups.

Our results were consistent with those of Welson et al. [13], who demonstrated that BCL2 immunohistochemical expression begins to decrease 24 hours postmortem and becomes negative by 96 hours. Also, Elias et al. [27] found that BCL2 levels were linearly related to PMI in their study of human skin. The steady decline in Bcl-2 expression is thought to be linked to two key factors: the cell's resistance to apoptosis and the degradation of cell-surface proteins due to the large number of circulating free radicals [27].

Regarding the significant results in our study, we performed a multivariate linear regression analysis. We found that the most important predictors of PMI were BCL2 and GSH in the spleen, pancreas, and heart. The best regression formula in our study PMI=97.434-2.838* BCL2 (Heart) -0.449* GSH (Spleen)

Ali & Ahmed [15] reported in their study that, in the prostate, the most significant predictor was MDA, followed by GSH, then SOD, and lastly NO. According to research by Welson et al. [13], the testis showed the strongest correlation with MDA, SOD, and GSH, which significantly impacted PMI prediction. Khalifa et al. [28] reported that the most effective regression formula was for skin tissue, with GSH, LDH, and MDA as the most significant variables influencing early PMI prediction.

Conclusion

PMI could be estimated from variations in oxidative stress markers (MDA, GSH, and SOD) in the spleen, pancreas, and heart. In the pancreas, MDA, GSH, and SOD showed strong positive associations with PMI. In the heart, GSH was positively associated with PMI. In the spleen, GSH showed a significant negative correlation with PMI, whereas SOD showed a strong positive correlation. In the heart, AIF demonstrated a highly significant negative correlation with PMI. (p-value <0.001) while the pancreas and spleen showed a non-significant correlation. Histopathological changes in tissues after death were time-dependent and could be used to estimate PMI. BCL2 immunohistochemical staining showed a progressive decline in staining intensity over time after death and strong negative correlations with PMI across all tissues; it is a useful parameter for estimating PMI. Four novel equations were developed to estimate PMI using the studied parameters across different organs.

Acknowledgment

None.

Funding

None.

Conflicts of Interest

The authors report there are no competing interests to declare.

References

[1] Thakral S, Purohit P, Mishra R, Gupta V, Setia P. The impact of RNA stability and degradation in different tissues to the determination of postmortem interval: A systematic review. Forensic Sci Int. 2023;111772. [DOI: 10.1016/j.forsciint.2023.111772]

[2] Elghamry HA, Hassan FM, Mohamed MI, Abdelfattah DS, Abdelaal AG. Estimation of the postmortem interval using GAPDH mRNA in skin and heart tissues of albino rats at different environmental conditions. Egypt J Forensic Sci. 2018;8:1-6. [DOI: 10.1186/s41935-018-0059-3]

[3] Brooks JW. Postmortem changes in animal carcasses and estimation of the postmortem interval. Vet Pathol. 2016;53(5):929-40. [DOI: 10.1177/0300985816629720]

[4] Lv YH, Ma KJ, Zhang H, He M, Zhang P, Shen YW, et al. A time course study demonstrating mRNA, microRNA, 18S rRNA, and U6 snRNA changes to estimate PMI in deceased rat spleen. J Forensic Sci. 2014;59(5):1286-94. [DOI: 10.1111/1556-4029.12470]

[5] Pasaribu RS, Auerkari EI, Suhartono AW. Histological changes in oral mucosa (gingiva) as a method for estimating postmortem interval: A literature review. Saudi Dent J. 2024. [DOI: 10.1016/j.sdentj.2024.05.002]

[6] El-Noor MM, Elhosary NM, Khedr NF, El-Desouky KI. Estimation of early postmortem interval through biochemical and pathological changes in rat heart and kidney. Am J Forensic Med Pathol. 2016;37(1):40-6. [DOI: 10.1097/PAF.0000000000000213]

[7] Kiernan JA. Staining, histochemistry and histotechnology FAQ. [Link]

[8] Suvarna KS, Layton C, Bancroft JD. Bancroft's theory and practice of histological techniques. 8th ed. Elsevier; 2018. [DOI: 10.1016/C2015-0-00143-5]

[9] Chan YH. Biostatistics 102: Quantitative data – parametric & non-parametric tests. Singapore Med J. 2003;44(8):391-6. [Link]

[10] Chan YH. Biostatistics 104: Correlational analysis. Singapore Med J. 2003;44(12):614-9. [Link]

[11] Chan YH. Biostatistics 201: Linear regression analysis. Singapore Med J. 2004;45(2):55-61. [Link]

[12] Zaki AR, Tohamy AF, Yaseen NE. Estimation of postmortem intervals by some biochemical changes and DNA degradation in rat brain and skeletal muscle tissues. Mansoura J Forensic Med Clin Toxicol. 2017;25(1):59-78. [Link]

[13] Welson NN, Gaber SS, Batiha GE, Ahmed SM. Evaluation of time passed since death by examination of oxidative stress markers, histopathological, and molecular changes of major organs in male albino rats. Int J Legal Med. 2021;135:269-80. [DOI: 10.1007/s00414-020-02428-4]

[14] Shaaban DA, Farrag DI, Bayoumy A, Saad E. Estimation of early postmortem interval by biochemical changes in brain and liver of rats using some oxidant and antioxidant parameters. Egypt J Forensic Sci Appl Toxicol. 2017;17(1):147-62. [Link]

[15] Ali D, Ahmed M. Prostatic estimation of time passed since death: Oxidative stress markers, histological and immunohistochemical examination (an experimental study). Ain Shams J Forensic Med Clin Toxicol. 2023;40(1):22-33. [DOI: 10.21608/ajfm.2023.295402]

[16] Mostafa HE, El-Shafei DA, Abouhashem NS, Alaa El-Din EA. Could skeletal muscle changes provide a reliable method for estimating the time since death: A histological, biochemical, and DNA study. Aust J Forensic Sci. 2023;55(1):46-58. [DOI: 10.1080/00450618.2021.1964975]

[17] Hegazy AM, Nasr SM, Aziem SH. Ultrastructure of cerebral cortex investigation during early postmortem changes in a rat model. Indian J Forensic Med Pathol. 2020;13(3):210-8. [Link]

[18] da Fonseca CA, Paltian J, Dos Reis AS, Bortolatto CF, Wilhelm EA, Luchese C. Na+/K+-ATPase, acetylcholinesterase and glutathione S-transferase activities as new markers of postmortem interval in Swiss mice. Leg Med (Tokyo). 2019;36:67-72. [DOI: 10.1016/j.legalmed.2018.11.005]

[19] Su SB, Motoo Y, Xie MJ, Mouri H, Asayama K, Sawabu N. Superoxide dismutase is induced during rat pancreatic acinar cell injury. Pancreas. 2002;24(2):146-52. [DOI: 10.1097/00006676-200203000-00008]

[20] Estaras M, Martinez-Morcillo S, García A, Martinez R, Estevez M, Perez-Lopez M, et al. Pancreatic stellate cells exhibit adaptation to oxidative stress evoked by hypoxia. Biol Cell. 2020;112(10):280-99. [DOI: 10.1111/boc.201900073]

[21] Zheng W, Huang LZ, Zhao L, Wang B, Xu HB, Wang GY, et al. Superoxide dismutase activity and malondialdehyde level in plasma and morphological evaluation of acute severe hemorrhagic shock in rats. Am J Emerg Med. 2008;26(1):54-8. [DOI:

10.1016/j.ajem.2007.02.012]

[22] Peng D, Lv M, Li Z, Tian H, Qu S, Jin B, et al. Postmortem interval determination using mRNA markers and DNA normalization. Int J Legal Med. 2020;134:149-57. [DOI: 10.1007/s00414-019-02116-3]

[23] Bai X, Peng D, Li Z, Tian H, Zhang L, Yang D, et al. Postmortem interval (PMI) determination by profiling of HAF mRNA degradation using RT-qPCR. Forensic Sci Int Genet Suppl Ser. 2017;6:182-3. [DOI: 10.1016/j.fsigss.2017.09.073]

[24] Öztürk C, Şener MT, Şener E, Yılmaz İ, Akcay F, Süleyman H. The investigation of damage in muscle tissue with oxidant/antioxidant balance and the extent of postmortem DNA damage in rats. Life Sci J. 2013;10(3):1631-7. [Link]

[25] Tomita Y, Nihira M, Ohno Y, Sato S. Ultrastructural changes during in situ early postmortem autolysis in kidney, pancreas, liver, heart and skeletal muscle of rats. Leg Med (Tokyo). 2004;6(1):25-31. [DOI: 10.1016/j.legalmed.2003.08.002]

[26] Mohamed A, Elbohi K, Sharkawy N, Hassan M. Biochemical and apoptotic biomarkers as indicators of time elapsed since death in experimentally induced traumatic brain injury. SM J Forensic Res Criminol. 2017;1(2):1-7. [Link]

[27] Elias EZ, Osman K, Aziz SM, Mohamed J, Mansar AH, Ibrahim SF. Determination of time of death based on basic histological stain and immunostain changes. J Sains Kesihat Malays. 2004;2:63-70. [Link]

[28] Khalifa FN, Hosny SA, Moawad AM. Histobiochemical changes in early postmortem interval in liver, pancreas, skin and kidney of adult male albino rats. Rechtsmedizin. 2022;32(5):374-85. [DOI: 10.1007/s00194-022-00554-2]